This document is the Accepted Manuscript version of a Published Work that appeared in final form in Journal of Materials Chemistry A , copyright © Royal Society of Chemistry after peer review and technical editing by thepublisher. To access the final edited and published work see http://pubs.rsc.org/en/content/articlelanding/2015/ta/c5ta01632k#!divAbstract

High Photocurrent in Oligo-thienylenevinylene Based Small Molecule Solar Cells Having 4.9% Solar-to-Electrical Energy Conversion.

Núria F. Montcada ; Rocío Domínguez ; Beatriz Pelado ; Pilar de la Cruz ; Emilio Palomares ; Fernando Langa

A set of five novel oligo-thienylenevinylene organic molecules have been synthesized and characterized for use as electron donor moieties in bulk-heterojunction solution-processed organic solar cells combined with PC71BM as an electron acceptor. The results show a broad range of solar-to-electrical conversion efficiencies, with values up to 4.9% achieved with a photocurrent value as high as 12 mA cm–2 under standard measurement conditions. Moreover, another aim of this study was to determine the main limiting processes that control the final performance parameters of these devices. Photo-induced charge transfer measurements, such as charge extraction (CE), Transient Photo-Voltage (TPV) and mobility measurements, were carried out in order to determine the main loss mechanisms and to correlate them with the electron donor molecular design.

Keywords: small molecule, organic solar cells, charge recombination, charge extraction, high photocurrent.

Introduction

Fundamental research in organic solar cells based on solution processed semiconductor molecules (so called solution processed small molecule solar cells, smOSC) has attracted considerable attention due to the increase in the device efficiency upon sun-simulated irradiation. Novel synthetic strategies for the electron donor molecules, as well as, the film nanomorphology optimization have lead to new "champion" cells with published efficiencies near 10% for single junction[1] devices.

The use of small molecules is a constant growing field because it presents several advantages in comparison with semiconductor polymers, such as reproducibly synthesis, high degree of purity, easy up-scaling among others[2-5]; However, several uncertainties are still unsolved, for example the molecular design and their correlation with the final device performance.[6-10]

We further present in this work a complete study of a novel set of small molecules build around a 3,4-ethylenedioxythiophene (EDOT) group and based on the previously published work about **smL01**.[11] All these molecules present a higher symmetric molecular architecture of Acceptor-π-Donor-π-Acceptor (A-π-D-π-A) in order to favour a solid-state packing[12]. One the other hand, we consider this approach as one of the most promising strategies for molecular band-gap tuning, an effective interaction between intercalating electron-rich donors and electron-deficient acceptors reduce the optical band-gap, and definitely, tune the HOMO and LUMO energy levels to maximize the intermolecular charge transfer. On the other hand, the presence of the π-bridge groups, branched thienylenevinylenes in our case, improves intra-molecular π-delocalization. Moreover, the carriers mobilities in the organic blend are one of the major limiting processes for the smOSC-based devices efficiencies and is generally reflected in their low fill factors (FF).[8, 13] Thus, a selection of a proper acceptor moiety is also very important because of their role within the electron donor molecule to improve hole mobility. Furthermore, it is important that the acceptor is strong enough to pull the maximum of electrons from the donor, hence, increasing the absorption capability of the donor moiety; however, the main drawback of this strategy is that choosing a too strong acceptor may also decrease the hole mobility, or shift the LUMO impeding charge dissociation.[14, 15]

In the work described here we analysed and compared all of the aspects discussed above and evaluated their effects on the final device characteristics, with the results compared with those obtained in our previous[11] study using **smL01**. The effect of increasing the number of thienylenevinylene units, two thienylenevinylene (**smL02**) and three thienylenevinylene (**smL03**) units per side, was studied in order to determine the effect of the intramolecular π-delocalization and the effect on the absorption capability of the donor moiety. In addition, the removal of one of the alkyl chains of the thiophene (**smL04** and **smL06**) was studied to provide information about the real role of these pendant groups both morphological and energetically. Finally, a direct comparison was made between two different acceptor moieties, dicyanovinylene (DCV) and rhodanine (Rho) (**smL04** and **smL06**), with the latter being a less electrophilic compound. This strategy was investigated with the aim of determining the effect of the strength of the acceptor moiety and the repercussions that this has on the transport properties within the molecule. The molecular structures of the molecules used in this study are shown in Scheme 1.

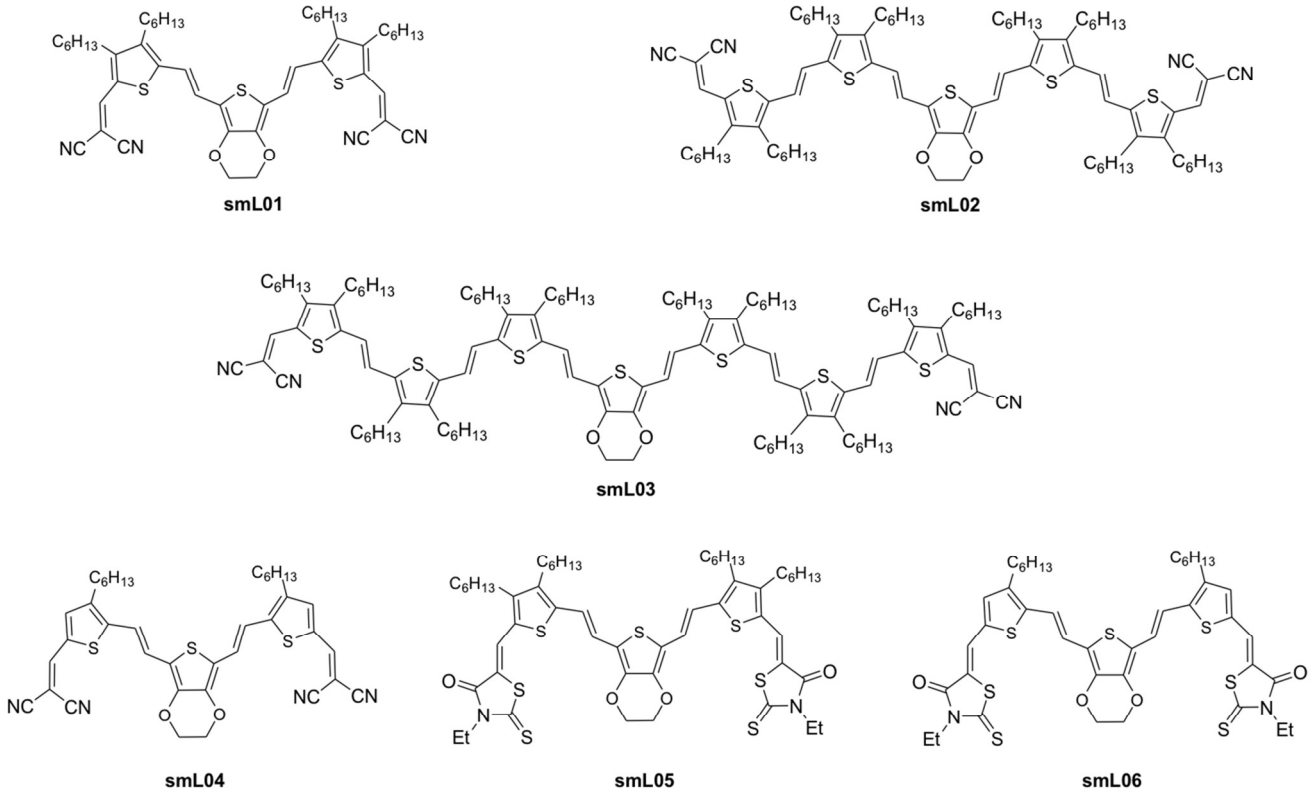

Scheme 1. Chemical structures for **smL01-06**.

Results and discussion

Synthesis, photochemical and electrochemical characterization of the molecules.

Synthesis of **smL04** and **smL06** started from bisaldehyde 5a, **smL05** was prepared from bisaldehyde **5b** while the synthesis of **smL02** and **smL03** will be described elsewhere. Bisaldehyde **5a** was synthesized according to **Scheme 2** starting from 2-formyl-3-hexylthiophene **1** by quantitative reduction with sodium borohydride, followed by zinc bromide mediated Michaelis-Arbuzov reaction of **2** to give phosphonate **3** (84% yield). Horner-Emmons reaction of **3** with 2,5-bisformyl-3,4-ethylendioxythiophene afforded **4** in 36% yield. Finally, Vilsmeier formylation of **4** yielded **5a** in 73% yield. The synthetic approach to **smL04**, **smL05** and **smL06** is depicted in **Scheme 3**. The Knoevenagel condensation of 5a with malononitrile provided the dicyanovinylene (DCV)-capped derivative **smL04** in 70% yield and Knoevenagel condensation of **5a-b** with 3-ethylrhodanine allowed us to obtain **smL05** and **smL06** (69% and 62% yields respectively).

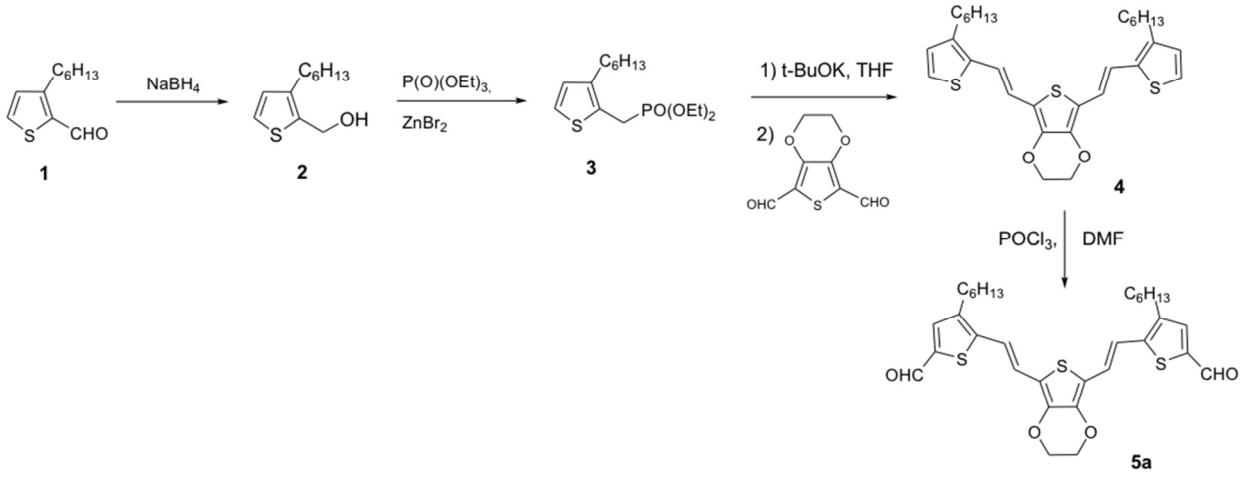

 This journal is © The Royal Society of Chemistry [year]

Scheme 2. Synthetic pathway to **5a**.

All compounds were characterized by ^{1}H, ^{13}C, NMR, FT-IR and MALDI-TOF MS spectral analysis to prove the structures (see SI). In all cases, the E configuration of the double bond were confirmed by coupling constants in the order of 15 Hz.
Thermogravimetric analysis (TGA) suggests that **smL04-06** exhibit good stability with decomposition temperature (Td) greater than 320 ºC under N_2 atmosphere (see SI, Figures S24-26).

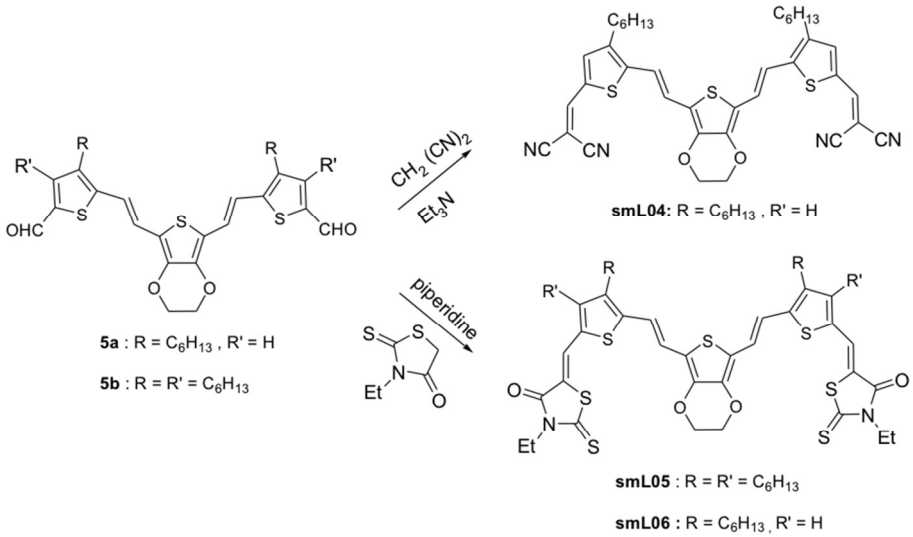

Scheme 3. Synthetic pathway to **smL04-06**.

The absorption spectra of oligomers **smL01**–**06** measured in dichloromethane are shown in Fig. 1 and the data are summarized in Table 1. Transformation of the formyl moieties to dicyanovinylene groups in **smL01** and **smL04** led to a red- shift in the lowest energy absorption band to 618 nm and 611 nm, respectively. These bands are ascribed to a charge transfer transition due to the donor−acceptor interactions between the electron-rich inner part of the molecule (EDOT) and the electron-deficient peripheral part (dicyanovinylene moieties). On the other hand, replacement of the aldehyde groups with 3- ethylrhodanine led to a stronger red-shift (to 632 nm and 622 nm, respectively) for derivatives **smL05** and **smL06** and this is due to the extension of the conjugation. For compounds **smL02** and **smL03**, the increased length of the π-conjugated system yielded red-shifted absorptions with maxima at 646 nm and 647 nm, respectively, with a tail on the absorption at around 800 nm. It should be noted that the extension of the conjugation from **smL02** to **smL03** caused a red-shift of only 1 nm, indicating that the saturation limit had been reached.
All of these new compounds have low optical band-gaps, in the range 1.75–1.87 eV, with the lower values corresponding to the compounds with a higher HOMO, **smL02** and **smL03**, due to the extension of the conjugation.

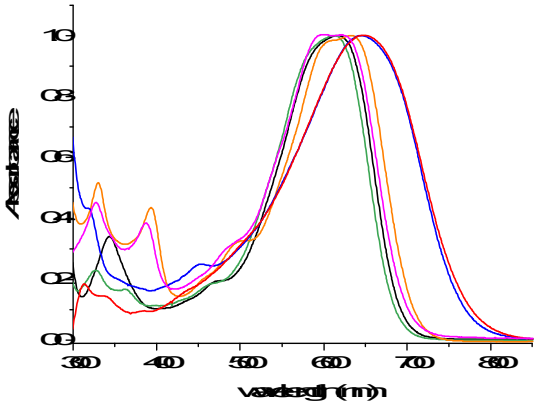

Figure 1. Normalized UV-vis spectra of **smL01 (—),smL02 (—),smL03 (—),smL04 (—),smL05 (—),smL06 (—)**,in CH_2Cl_2 ([ ] ≈ 2.5 10^{-6} M).

The oxidation potentials of **smL01-06** were investigated through Osteryoung Square Wave Voltammetry (OSWV) in o-dichlorobenzene/acetonitrile 4:1 solutions under argon (**Table 1**, Figures S29-S34) in order to determine the energy level of the HOMOs

of the newly synthesized materials as the alignment of the HOMO values are of high importance to achieve high open circuit voltage (V_{oc}), as this energy is closely related to the energy difference between the HOMO of an electron-donating material and the LUMO of an electron-accepting material. **smL01** and **smL04,** with dicyanovinylene groups as terminal acceptor units, show the lower HOMO values and they should give the larger V_{oc} values in PV devices (*vide infra*).

Table 1. Optical and electrochemical parameters of **smL01-06** compounds

Molecule	λ_{abs} *(nm)*	*log* ε	λ_{em} *(nm)*[a]	E_{ox1}[b] *(V)*	$E_{0\text{-}0}$[c] *(eV)*	*HOMO*[d] *(eV)*	*LUMO*[e] *(eV)*
smL01	618	4.87	709	0.50	1.87	-5.60	-3.73
smL02	646	4.85	796	0.16	1.76	-5.26	-3.50
smL03	647	5.21	784	-0.07	1.80	-5.03	-3.23
smL04	611	4.89	704	0.52	1.88	-5.62	-3.74
smL05	632	4.86	727	0.31	1.82	-5.41	-3.59
smL06	622	4.97	722	0.31	1.84	-5.41	-3.57

[a] Excitation at maximum wavelength. [b] OSWV (Osteryoung square wave voltammetry) value. [c]Optical value. [d]Calculated according to the equation: E_{HOMO}= -5.1-$E_{ox1(OSWV)}$. [e] Calculated according to the equation: E_{LUMO}= E_{HOMO}+ $E_{0,0}$ (eV).

Theoretical Calculations.

To gain insight into the geometrical, electronic, and optical properties of **smL01-06** we carried out quantum chemical calculations. The ground-state geometries of these molecules were fully optimized by the density functional (DFT) at B3LYP 6-31G* level *in vacuo* with Gaussian 03W. The optimized geometry, electron density distribution of HOMO and LUMO of **smL01-06** are shown in Figure S34. In all cases, the calculated ground-state geometries reveal an almost planar conformation of the conjugated system[16] (dihedral angles ≈ 1-2º), with the acceptor unit, dicyanovinylene or 3-ethylrhodanine, *cis* to the thiophene S-atom. This planar conformation must favour the π-π stacking between the molecular backbones. In those molecules with 3-ethylrhodanine as acceptor unit (**smL05** and **smL06**), two possible conformations, **smL05-A** and **smL05-B** (Scheme S1), were calculated being **smL05-A**, facing both sulphur atoms, more stable than **smL05-B**, according with that found for related compounds.[17] It should be indicated that, in **smL05-A**, the distance between both sulphur atoms is 3.27 Å, lower than the sum of the Van der Waals radio (3.70 Å), suggesting the existence of through space non-bonding interactions between them.

It is very useful to determine the electronic distribution of the HOMO and LUMO levels as they give information about the photovoltaic properties of the involved molecules. The electron density of the HOMO for all molecules is mainly distributed not only on the EDOT central unit and the oligothienylenevinylene backbone, whereas that of the LUMO is mainly localized on the terminal acceptor groups and the adjacent thienylenevinylene units. The calculated band gap is around 2 eV for those molecules with three thiophene rings (**smL01** and **smL04-06**), being significantly lower for **smL02** and **smL03** (ΔE = 1.63 and 1.50 eV respectively, figure S37) due to the more extended conjugation in these systems, in reasonable good agreement with the experimental values.

Organic film characterization.

The molecules were deposited over a substrate using conditions determined from the optimization studies (See SI); the absorbance in the film was measured for each pristine molecule and blended with fullerene and the light harvesting efficiencies (LHE) were calculated using **Equation 1** and shown in **Figure 2**.

Equation 1 $\mathbf{LHE=1-10^{-abs(\lambda)}}$

The **smL01** is the molecule with the highest LHE peak (65%) at λ=690 nm; the other molecules were deposited under same processing conditions. In case of **smL02** and **smL03** is clear that the increase of each thienylenevinylenes group favors a wider and a shifted absorption spectra to the red (bathochromic shift). For **smL04** the LHE is slightly below **smL01** and also a shift towards longer wavelengths was observed. **smL05** and **smL06** Rho-based molecules present a LHE below the values observed for **smL01-04** pointing that the Rho substitution leads to a weaker CT bands.

 This journal is © The Royal Society of Chemistry [year]

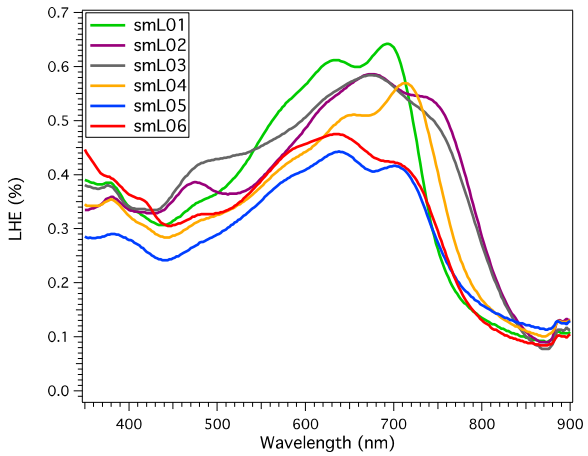

Figure 2. Light harvesting efficiency (LHE) for all **smL** molecules blended with $PC_{71}BM$. The films are 75 nm thick.

Characterization of organic solar cells.

Complete devices were fabricated following the optimized conditions and characterized by IV measurements; the optimized cell of each set is shown in **Figure 3** and their main performance parameters are shown in **Table 2**.

The results obtained in this study, for the **smL01** molecule, are in good agreement with our previous work; even though, for this work a new batch of **smL01** was synthesized. The **smL02** and **smL03** present lower photocurrent values as the number of thienylenevinylenes in the backbone increase; that lead us to start thinking about a direct relationship between the number of thiophenes and an important increase of the free charges recombination as we discuss later on this work. Taking into account previous studies, the presence of the alkyl chains at both sides of the molecule disfavors proper π-π interaction impeding inter-chain charge hopping.[3, 13, 17]

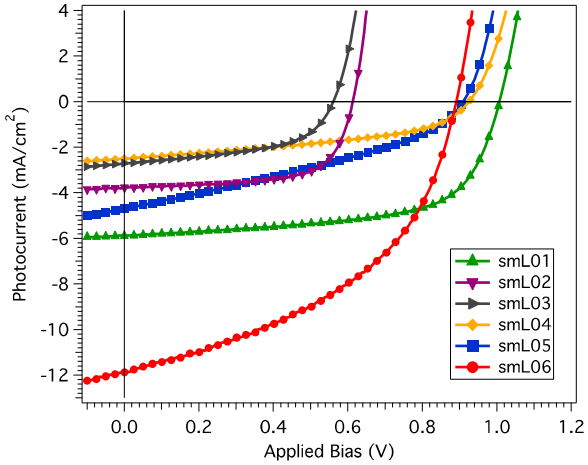

Figure 3 Photocurrent *vs* voltage (IV) curves for optimized **smL:$PC_{71}BM$** solar cells at 1 sun (sun simulated 100 $mWcm^{-2}$ light intensity).

Moreover, the lower V_{oc} observed for **smL02** and **smL03** compared to **smL01**, drops because of the difference of the HOMO energy level. Additionally, after EQE measurements shown in **Figure 4** we could appreciate a great reduction of the IPCE spectra in agreement to the measured photocurrent from the IV curves.

Table 2. Main performance parameters for optimized organic solar cells using **smL:$PC_{71}BM$** bulk-heterojunction 75 nm thick films.

Device	*Jsc (mA/cm^2)*	*Voltage (mV)*	*Fill Factor (%)*	*PCE (%)*
smL01	5.85	1000	63.70	3.7
smL02	3.78	613	66.43	1.5
smL03	2.70	562	52.61	0.8
smL04	2.50	924	45.43	1.1
smL05	4.70	910	34.91	1.5
smL06	11.98	890	45.69	4.9

J_{sc}=Short-circuit current density; V_{oc}=Open-circuit voltage; FF=Fill factor; PCE=Photo-current efficiency. Devices have an active area of 9mm^2.

In case of **smL04** the changes on the hexyl groups at the molecular structure, clearly affects negatively the photocurrent with a subsequent decrease, and moreover, the decrease in V_{oc} is also related to this subtle change on the molecular structure.
The DCV acceptor group was substituted by a Rho in **smL05** and **smL06**; In **smL05** devices a reduction of the photocurrent accompanied by a steep reduction of the FF and also an slight decrease of the V_{oc} can be observed; part of this V_{oc} leakage occurs due to the difference from the HOMO energy level position (-5.41 eV); the poorer FF caused by nanomorphology variations of the active layer indicating that Rho does not present such as a crystalline domains as DCV-based molecules due to variations in intramolecular polarity[13] that impacts also in the final photocurrent. The reduction of this photocurrent starts with the limitation of the LHE shown before, less photons can be absorbed using the same thickness and also less photons are finally converted to external current as shown in **Figure 4.**
On the other hand, with **smL06** using the same optimized fabrication conditions a PCE of nearly 5% was obtained, and also with a highest photo-current of 12 mA cm^{-2}; indicating a better self-organization compared to **smL05**. Taking into account the external quantum efficiency results shown in **Figure 4**, **smL06** presents the highest incident photon-to-current efficiency. The CE results for all **smL** complete devices are shown in Fig. 5. The geometric capacitance was calculated using Equation 2.

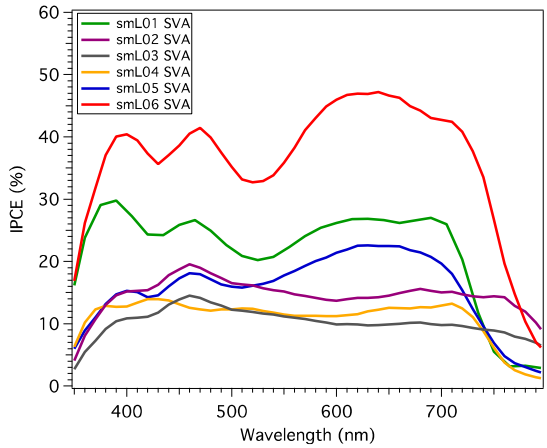

Figure 4. Incident Photon-to-Current Efficiency (IPCE) spectrum for the devices measured in **Figure 2**.

Equation 2 $$C_g = \frac{\varepsilon_0 \varepsilon_r A}{d}$$

Where C_g is the geometrical capacitance, which is related to the charge that the organic thin film has because is "sandwiched" between two metal electrodes. The ε_r is the dielectric constant for the organic material, which is estimated to be ≈ 3 for organic materials, the ε_0 is the dielectric constant that is 8.854 x 10^{-12} F m^{-1}, the A is the solar cell area (9 mm^2) and d is the film thickness (75 nm).
Considering that the solar cell area for all devices is equal and that the film thickness is also very much similar in all solar cells as measured by AFM type profilometer (75 nm) the Cg value has been calculated to be equal to 65 nF/cm^2.

This journal is © The Royal Society of Chemistry [year]

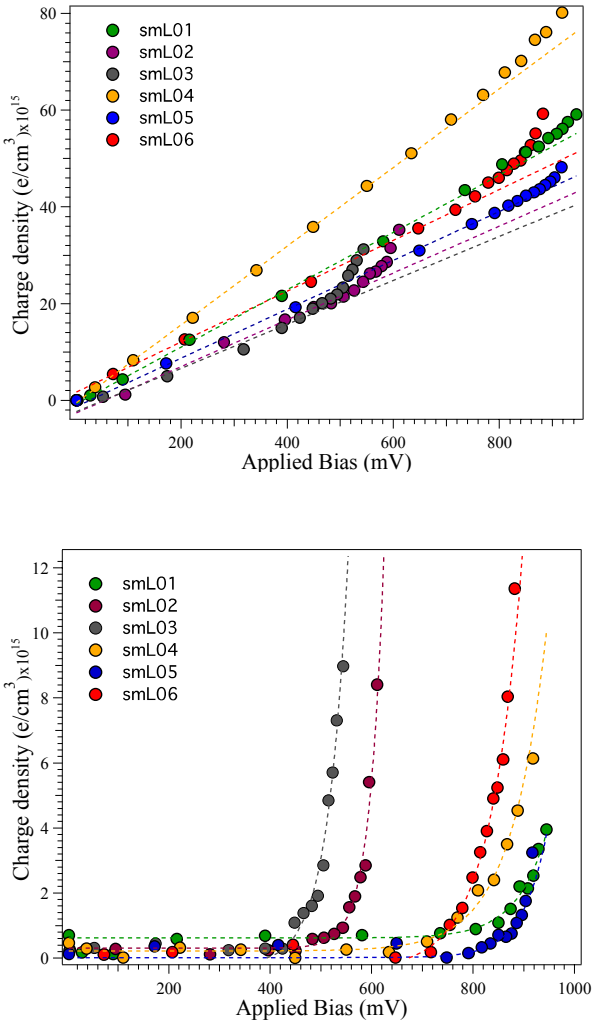

Figure 5. a) Total charge density at the solar cell under different light bias (solar cell voltage at different light illumination intensities) and b) Charge density after subtracting the geometrical capacitance (Equation 2).

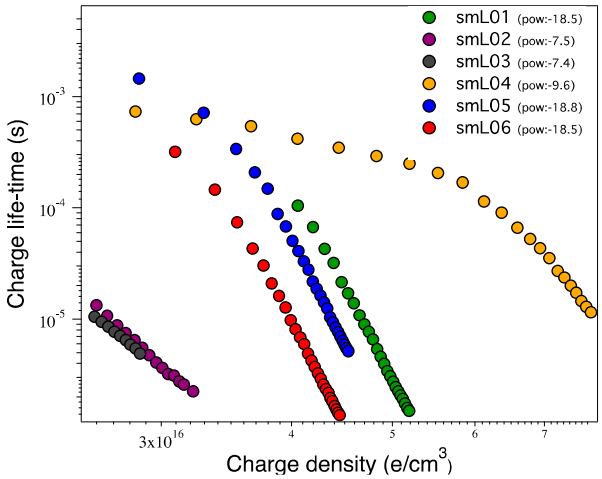

Figure 6. Charges lifetime of all organic solar cells measured in **Figure 2** under the same light bias as **Figure 4**. At the figure legend within parenthesis is the power law decay order after fitting the linear part of each curve.

Following CE measurements, we carried out transient photovoltage measurements [18-20] (TPV) measurements in order to determine and compare the different charge lifetimes for all of our; the points close to the V_{oc} at 1 sun conditions (in applied bias). These experimental points were fitted to a power-law exponential decay.
It can be seen in Figure 6 all molecules present similar decay orders indicating in all cases, far from second order. A recombination order close to 2 would mean that the measured kinetics correspond mainly to non-geminate bimolecular charge recombination reaction. For **smL02** and **smL03** are clearly the devices with faster recombination rates as the number of thienylenevinylenes increase at both side of the molecular backbone and particularly the non-geminate recombination is higher due to the location of the HOMO.

Finally, charge mobility measurements (Figure 7) were carried out measuring an IV curve of hole only devices for each **smL** molecule. The diode was forced to work at the space-charge-limited current (SCLC) conditions.
That plots were fitted to the Murgatroyd equation (Equation 3) that includes the effects of electric field and charge defects by the *Poole-Frenkle* factor.

Equation 3

$$J_{SCLC} = \frac{9}{8}\varepsilon\mu\frac{V_{eff}^2}{d^3}\exp\left(\frac{0.89\beta\sqrt{V_{eff}}}{\sqrt{d}}\right)$$

Where ε is the media permittivity, μ is the mobility, d the film thickness, β is the Poole-Frenkle factor and V_{eff} is the voltage ($V_{eff} = V_{oc} - V_{bi}$). All the mobility measurement results are listed in **Table 3.** The mobility measurements graphs can be found at the SI.

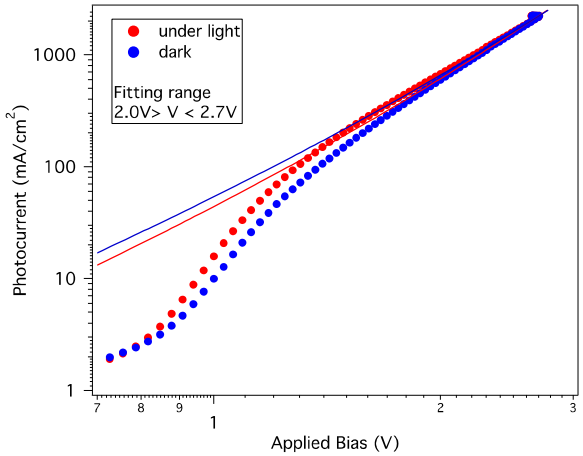

Figure 7. IV curves for a *hole only* device of **smL06:PC$_{71}$BM** bulk-heterojunction 75 nm thick film under sun simulated irradiation (100 mW cm^{-2}) and in the dark. The corresponding fitting is performed the voltage range at the figure legend.

Table 3. Hole mobility and *Poole-Frenkle* values for all **smL**:**PC$_{71}$BM** organic solar cells.

Device	*h^+ mobility ($Vcm^{-2}s^{-1}$)*	*β (Poole-Frenkle factor)*
smL01	$1.2\pm0.7\cdot10^{-6}$	$6.04\cdot10^{-3}$
smL02	$1.1\pm0.2\cdot10^{-5}$	$3.94\cdot10^{-3}$
smL03	$2.8\pm0.8\cdot10^{-5}$	$4.33\cdot10^{-3}$
smL04	$5.9\pm3.1\cdot10^{-7}$	$9.13\cdot10^{-3}$
smL05	$1.8\pm0.9\cdot10^{-4}$	$1.07\cdot10^{-3}$
smL06	$1.4\pm0.2\cdot10^{-5}$	$4.75\cdot10^{-3}$

Hole mobility results show a range of 3 orders of magnitude. Taking **smL01** as the reference, **smL02** and **smL03** present a noticeably increase of the mobility (from $x10^{-6}$ to $x10^{-5}$ $Vcm^{-2}s^{-1}$) as the number of thiophene groups and their respective alkyl chains increase; the effect of the alkyl chains is reflected in results of **smL04** where the absence of two of the alkyl chains retarded the hole mobility one order of magnitude (from $x10^{-6}$ to $x10^{-7}$ $Vcm^{-2}s^{-1}$). Moreover, the mobility of **smL05** and **smL06** are one and two orders of magnitude higher than **smL01**. The **smL05** presents the highest hole mobility that lead us to determine the remarkable contribution of the alkyl chains to the hole mobility.

This journal is © The Royal Society of Chemistry [year]

Experimental

Synthesis and characterization

Synthesis of 3-hexylthienylmethylphosphonate diethyl (3).
$NaBH_4$ (0.43 g, 11.4 mmol) was added portion wise to a solution of aldehyde **1** (1.12 g, 5.7 mmol) in 60 mL of 1:1 CH_2Cl_2/methanol. The mixture was stirred for 45 min, diluted with CH_2Cl_2 and washed with water. After extraction with CH_2Cl_2, the organic phase was dried over $MgSO_4$ and the solvent evaporated, yielding quantitatively the alcohol **2**, pure by TLC and ^{1}H NMR which was used in the next step without further purification.
Next, $ZnBr_2$ (1.5 g, 6.7 mmol) was added to a solution of the alcohol **2** (1.11 g, 5.6 mmol) and triethylphosphite (5 mL, 28 mmol) at room temperature, and stirred for 20 hours under argon. After consumption of the starting material (monitored by TLC), the reaction was poured over crushed ice containing conc. HCl, extracted with $CHCl_3$ and dried over $MgSO_4$. The solvent was removed under vacuum and the crude product was purified by column chromatography (silica-flash, hexane:ethyl acetate 3:2). Compound **3** was obtained as colourless oil in 84% yield (1.5 g, 4.7 mmol).
^{1}H-NMR (400 MHz, $CDCl_3$): δ/ppm: 7.13-7.11 (m, 1H), 6.85-6.84 (m, 1H), 4.10-4.03 (m, 4H), 3.31 (d, 2H, J = 20.8 Hz), 2.58-2.53 (m, 2H), 1.58-1.53 (m, 2H), 1.30-1.21 (m, 12H), 0.90-0.87 (m, 3H); ^{13}C-NMR (100 MHz, $CDCl_3$): δ/ppm: 140.8, 140.7, 128.6, 128.5, 125.7, 125.6, 123.2, 123.1, 62.4, 62.3, 31.8, 30.5, 30.4, 29.2, 28.4, 28.3, 27.0, 25.5, 22.6, 16.4, 16.3, 14.1; FT-IR (ATR): υ/cm^{-1}: 2928, 2858, 1254, 1053, 1022, 960, 725.

Synthesis of 4.
In a round-bottom flask, under argon atmosphere, 3-hexylthienylmethylphosphonate diethyl (**3**) (100 mg, 0.314 mmol) and 3,4-ethylendioxytiophendicarboxyaldehyde (28.3 mg, 0.143 mmol) were dissolved in dry THF (10 mL). At -78ºC, tBuOK (48.1 mg, 0.43 mmol) was added and the mixture stirred 2 hours at the same temperature. The yellow solution was extracted three times with diethylether. The organic phase was dried over $MgSO_4$, concentrated in vacuum and the obtained solid was purified by column chromatography (silica-flash, hexane:CH_2Cl_2 8:2). Compound **4** was obtained as a yellow solid in 36% yield (27 mg, 0.051 mmol).
^{1}H-NMR (400 MHz, CDCl3): δ/ppm: 7.07 (d, 2H, J = 4.8 Hz), 6.96 d, 2H, J = 15.6 Hz), 6.90 (d, 2H, J = 15.6 Hz), 6.84 (d, 2H, J = 4.8 Hz), 4.31 (s, 4H), 2.66 (t, 4H, J = 7.6 Hz), 1.60 (m, 4H), 1.34 (m, 12H), 0.91 (m, 6H); ^{13}C-NMR (100 MHz, $CDCl_3$) δ/ppm: 140.6, 139.3, 136.6, 129.8, 122.6, 118.0, 116.8, 115.3, 64.9, 31.7, 30.9, 29.0, 28.4, 22.6, 14.2; UV-vis (CH_2Cl_2) λ_{max}/nm (log ε): 436 (4.33), 328 (4.07); FT-IR (ATR): υ/cm-1: 2923, 2854, 1442, 1362, 1080, 933; MS (*m/z*) (MALDI-TOF): calculated for $C_{30}H_{38}O_2S_3$: 526.20; found 526.70 (M+).

Synthesis of 5a.
In a round-bottom flask, under argon atmosphere, $POCl_3$ (63 mg, 0.41 mmol) was added to a solution of **4** (48 mg, 0.091 mmol) and DMF (42 mg, 0.57 mmol) in dry dichloroethane (10 mL). The mixture was stirred overnight at room temperature. Afterwards, 1 M sodium acetate was added up to neutrality and then, the mixture was stirred vigorously for 1 h. The solution was extracted with dichloromethane and the organic phase dried over $MgSO_4$. After the evaporation of the solvent, the product was purified by column chromatography (silica-flash, hexane: CH_2Cl_2 1:1) to give compound **5a** as a red solid in 73% yield (39 mg, 0.07 mmol).
^{1}H-NMR (400 MHz, $CDCl_3$): δ/ppm: 9.80 (s, 2H), 7.51 (s, 2H), 7.15 (d, 2H, J = 15.6 Hz), 6.97 (d, 2H, J = 15.6 Hz), 4.35 (s, 4H), 2.68 (m, 4H), 1.63 (m, 4H), 1.35 (m, 12H), 0.92 (m, 6H); ^{13}C-NMR (100 MHz, $CDCl_3$) δ/ppm: 182.4, 147.0, 141.8, 140.9, 139.4, 138.9, 121.0, 117.5, 116.5, 65.0, 31.6, 30.5, 28.9, 28.3, 22.6, 14.1; UV-Vis (CH_2Cl_2) λ_{max}/nm (log ε): 479 (4.6), 382 (4.2); FT-IR (KBr) υ/cm-1: 2928, 2850, 1651, 1601, 1431, 1362, 1281, 1080, 930, 667; MS (*m/z*) (MALDI-TOF): calculated for $C_{32}H_{38}O_4S_3$: 582.19; found 582.30 (M+).

Synthesis of smL04.
In a round-bottom flask, under argon atmosphere, three drops of Et_3N were added to a solution of malononitrile (17 mg, 0.25 mmol) and bis-aldehyde **5a** (49 mg, 0.084 mmol) in $CHCl_3$ (10 mL). The reaction mixture was stirred at room temperature for 5 hours and washed with brine. The organic phase was dried over $MgSO_4$ and the solvent removed by evaporation under reduced pressure. After purification by column chromatography (silica-gel, n-hexane:CH_2Cl_2 1:1), compound **smL04** was obtained in 70% yield (40 mg, 0.06 mmol).
^{1}H-NMR (400 MHz, $CDCl_3$): δ/ppm: 7.66 (s, 2H), 7.43 (s, 2H), 7.21 (d, 2H, J = 15.6 Hz), 6.99 (d, 2H, J = 15. 6 Hz), 4.38 (s, 4H), 2.67 (t, 4H, J = 7.6 Hz), 1.56 (m, 4H), 1.34 (m, 12H), 0.91 (m, 6H); ^{13}C-NMR (100 MHz, $CDCl_3$): δ/ppm: 149.9, 149.5, 142.6, 141.8, 141.6, 132.1, 122.9, 117.7, 117.2, 114.7, 113.8, 75.0, 65.0, 31.5, 30.4, 28.9, 28.0, 22.6, 14.1; UV-Vis (CH_2Cl_2) λ_{max}/nm (log ε): 611 (4.9), 362 (4.1), 327 (4.2); FT-IR (KBr) υ/cm-1: 2930, 2860, 2210, 1560, 1410, 1280, 1080, 930; MS (*m/z*) (MALDI-TOF): calculated for $C_{38}H_{38}N_4O_2S_3$: 678.22; found 678.35 (M+).

General procedure for the synthesis of smL05 and smL06.
The corresponding bis-aldehyde, **5a** or **5b**, was dissolved in dry $CHCl_3$; three drops of piperidine and then 3-ethylrhodanine were added, and the resulting solution was refluxed for 12 h under argon. The reaction mixture was extracted with CH_2Cl_2, washed with brine, and dried over $MgSO_4$. After removal of solvent, the product was purified by column chromatography (silica gel, n-hexane:CH_2Cl_2 1:1).

Synthesis of smL06: From 0.07 mmol of **5a** and 0.21 mmol of 3-ethylrhodanine. **smL06** was obtained as a blue solid in 69% yield (41 mg, 0.047 mmol).

^{1}H-NMR (400 MHz, $CDCl_3$) δ/ppm: 7.77 (s, 2H), 7.16 (s, 2H), 7.10 (d, 2H, J = 15.6 Hz), 6.95 (d, 2H, J = 15.6 Hz), 4.39 (s, 4H), 4.19 (c, 4H, J = 6.8 Hz), 2.66 (t, 4H, J = 7.6 Hz), 1.63-1.59 (m, 4H), 1.35-1.20 (m, 18H), 0.92 (m, 6H); ^{13}C-NMR (100 MHz, $CDCl_3$) δ/ppm: 192.1, 167.3, 146.1, 142.8, 140.8, 137.3, 134.8, 125.1, 120.1, 120.0, 117.2, 116.9, 65.0, 39.9, 31.6, 30.6, 28.9, 28.2, 22.6, 14.1, 12.3; UV-Vis (CH_2Cl_2) λmax/nm (log ε): 622 (5.0), 387 (4.6), 327 (4.6); FT-IR (KBr) υ/cm^{-1}: 2930, 2860, 1700, 1570, 1420, 1230, 1120, 879; MS (*m/z*) (MALDI-TOF): calculated for $C_{42}H_{48}N_2O_4S_7$: 868.17; found 868.39 (M+).

Synthesis of smL05: From 0.05 mmol of **5b** and 0.14 mmol of 3-ethylrhodanine. **smL05** was obtained as a blue solid in 62% yield (30 mg, 0.03 mmol).
^{1}H-NMR (400 MHz, $CDCl_3$) δ/ppm: 7.90 (s, 2H), 7.12 (d, 2H, J = 15.6 Hz), 6.98 (d, 2H, J = 15.6 Hz), 4.40 (s, 4H), 4.20 (c, 4H, J = 6.8 Hz), 2.71 (t, 4H, J = 7.6 Hz), 2.62 (t, 4H, J = 7.6 Hz), 1.52 (m, 8H), 1.42-1.29 (m, 30H), 0.93-0.91 (m, 12H); ^{13}C-NMR (100 MHz, $CDCl_3$) δ/ppm: 192.4, 167.5, 150.7, 145.9, 141.9, 140.9, 130.7, 123.8, 120.0, 119.0, 117.6, 117.0, 65.02, 39.9, 31.8, 31.6, 31.5, 31.0, 29.4, 29.3, 27.6, 27.0, 22.6, 14.2, 14.1, 12.4; UV-vis (CH_2Cl_2) λ_{max}/nm (log ε): 632 (4.9), 393 (4.5), 330 (4.6); FT-IR (KBr) υ/cm-1: 2920, 2850, 1700, 1570, 1320, 1230, 1130, 1080, 879; MS (*m/z*) (MALDI-TOF): calculated for $C_{54}H_{72}N_2O_4S_7$: 1036.35; found 1036.52 (M+).

Device fabrication and characterization

Pre-patterned Indium Tin Oxide (ITO) 5 Ohm/square sodalime glass substrates were first rinsed with acetone to remove the residual photoresist layer. The substrates were then placed in a Teflon holder and sequentially sonicated in acetone (1 × 10 min) and isopropanol (2 × 10 min), and finally dried under a nitrogen flow. The ITO substrates where ozone-treated in a UV-ozone cleaner for 30 min in ambient atmosphere, and subsequently coated in air with a layer of filtered (0.45 μm, cellulose acetate) solution of Poly(3,4-ethylenedioxythiophene):poly(styrenesulfonate) (4500 rpm 30 seconds followed by 3500 rpm 30 seconds). The PEDOT:PSS film was dried at 120 ºC under inert atmosphere for 15 min. Active layers were spin-coated (8000 rpm) in air over the PEDOT:PSS layer from a 20 mg/ml (total concentration) solution of donor derivative and $PC_{71}BM$ with a ratio 1:2 in weight. The solvent annealing step was carried out straight after deposition of the active layer by exposing the films to a saturated vapor atmosphere of dichloromethane in a controlled volume closed vessel. The vessel (100 ml) was filled with 10 ml of CH_2Cl_2 and left sealed for 5 min prior to the SVA step to ensure the saturation of the atmosphere. The substrates were exposed to the solvent vapours from 1 to several minutes by placing them into the solvent vessel.

The cathode layer was deposited by thermal evaporation in an ultra high vacuum chamber ($1\cdot 10^{-6}$ mbar). Metals were evaporated through a shadow mask leading to devices with an area of 9 mm^2. LiF (0.6 nm) and Al (80 nm) were deposited at a rate of 0.1 Å/s and 0.5-1 Å/s respectively. Following fabrication, the films were maintained under a nitrogen atmosphere and stored in the dark until used. In the case of hole only and electron only devices the solar cells were prepared as explain above but for hole only devices the structure was ITO/PEDOT:PSS/donor:$PC_{71}BM$/Au and for electron only devices the structure was ITO/ZnOnp/donor:$PC_{71}BM$/Al. All device efficiencies values correspond to masked devices with an active area of 9 mm^2.

The UV-Vis absorption spectra of films were measured using a Shimadzu UV-1700 spectrophotometer. The J-V characteristics of the devices were measured using a Sun 2000 Solar Simulator (150 W, ABET Technologies). The illumination intensity was measured to be 100 mW cm^{-2} with a calibrated silicon photodiode (NREL). The appropriate filters were utilized to faithfully simulate the AM 1.5G spectrum. The applied potential and cell current were measured with a Keithley 2400 digital source meter. The current to voltage (IV curve) was plotted automatically with a home-built Labview© software. The thickness of the films was measured with a stylus profilometer Ambios Tech. XP-1, from a scratch made in the middle of the film.

Conclusions

In conclusion we have designed and synthesized a series of organic semiconductor molecules based on the EDOT unit as a donor moiety for small molecule solution processed bulk heterojuntion solar cells achieving efficiencies of 4.9% under standard simulated illumination conditions. The **smL01** molecule presents the highest light harvesting efficiency (65%), however, it is demonstrated that all devices performances are mainly limited by lower mobility limiting the fabrication of the solar cells to very thin active layers. The increase of the thiophenes units and the use of alkyl chains broadens the absorption spectra to the red and allows higher fill factors (FF) in the solar cells, as observed for **smL02** and **smL03**, however, we observe an increase in charge recombination too. In the TPV measurements both, **smL02** and **smL03** present higher recombination rates compared to the other members of the **smL** family; Thus, it seems that thiophene units increase the hole mobility but also increases charge recombination. Finally, **smL06** presents the highest efficiency and an outstanding photocurrent of 12 mA cm^{-2}; the main reason is the higher internal conversion efficiency of the device as reflected by the highest IPCE value despite not presenting the highest LHE and not having the best hole mobility values.

Acknowledgements

We would like to thank *MINECO* for the projects CTQ2013-47183-R and CTQ2013-48252-P. EP thanks the support through Severo Ochoa Excellence Accreditation 2014-2018(SEV-2013-0319). RD thanks to *Ministerio de Educación, Cultura y Deporte* of Spain for a FPU grant and BP thanks to *MINECO* for a FPI grant.

 This journal is © The Royal Society of Chemistry [year]

Notes and references

[a]*Institute of Chemical Research of Catalonia (ICIQ), Avinguda del Països Catalans 16, 43007 Tarragona, Spain. Fax: +34 977 920 823; Tel: +34 977 920 200; E-mail: epalomares@iciq.es*
[b] Institute for Nanoscience, Nanotechnology and Molecular Materials (INAMOL). University of Castilla-la Mancha, Campus de la Fábrica. 45071. Toledo, Spain. E-mail: *Fernando.Langa@uclm.es*
[c]*Catalan Institution for Research and Advanced Studies (ICREA), Passeig de Lluis Companys 23, 08010 Barcelona, Spain*
[+]*These authors contributed equally to this work.*

† Electronic Supplementary Information (ESI) available: [. See DOI: 10.1039/b000000x/

1. B. Kan, Q. Zhang, M. Li, X. Wan, W. Ni, G. Long, Y. Wang, X. Yang, H. Feng and Y. Chen, *J. Mat. Chem.*, 2014, **136**, 15529.
2. J. Peet, J. Y. Kim, N. E. Coates, W. L. Ma, D. Moses, A. J. Heeger and G. C. Bazan, *Nat. Mater.*, 2007, **6**, 497-500.
3. G. C. Welch, L. A. Perez, C. V. Hoven, Y. Zhang, X.-D. Dang, A. Sharenko, M. F. Toney, E. J. Kramer, T. Q. Nguyen and G. C. Bazan, *J. Mat. Chem.*, 2011, **21**, 12700.
4. A. K. K. Kyaw, D. H. Wang, V. Gupta, J. Zhang, S. Chand, G. C. Bazan and A. J. Heeger, *Adv. Mater.*, 2013, **25**, 2397-2402.
5. M. Chandrasekharam, M. Anil Reddy, K. Ganesh, G. D. Sharma, S. Prakash Singh and J. Laxmikanth Rao, *Org. Elec.*, 2014, **15**, 2116.
6. H. Bürckstümmer, N. M. Kronenberg, M. Gsänger, M. Stolte, K. Meerholz and F. Würthner, *J. Mat. Chem*,, 2010, **20**, 240-243.
7. H. Bürckstümmer, E. V. Tulyakova, M. Deppisch, M. R. Lenze, N. M. Kronenberg, M. Gsänger, M. Stolte, K. Meerholz and F. Würthner, *Angew. Chem. Int. Ed.*, 2011, **50**, 11628-11632.
8. N. M. Kronenberg, V. Steinmann, H. Bürckstümmer, J. Hwang, D. Hertel, F. Würthner and K. Meerholz, *Adv. Mater.*, 2010, **22**, 4193-4197.
9. S.-W. Chiu, L.-Y. Lin, H.-W. Lin, Y.-H. Chen, Z.-Y. Huang, Y.-T. Lin, F. Lin, Y.-H. Liu and K.-T. Wong, *Chem. Comm*, 2012, **48**, 1857-1859.
10. Y.-H. Chen, L.-Y. Lin, C.-W. Lu, F. Lin, Z.-Y. Huang, H.-W. Lin, P.-H. Wang, Y.-H. Liu, K.-T. Wong, J. Wen, D. J. Miller and S. B. Darling, *J. Am. Chem. Soc.*, 2012, **134**, 13616-13623.
11. N. F. Montcada, B. Pelado, A. Viterisi, J. Albero, J. Coro, P. de la Cruz, F. Langa and E. Palomares, *Org. Electron.*, 2013, **14**, 2826-2832.
12. H. Bürckstümmer, N. M. Kronenber, M. Gsänger, M. Stolte, K. Meerholz and F. Würthner, *J. Mat. Chem.*, 2010, **20**, 240-243.
13. W. Wu, Y. Liu and D. Zhu, *Chem. Soc. Rev.*, 2010, **39**, 1489-1502.
14. B. Kim, X. Ma, C. Chen, Y. Ie, E. W. Coir, H. Hashemi, Y. Aso, P. F. Green, J. Kieffer and J. Kim, *Adv. Funct. Mater.*, 2013, **23**, 439-445.
15. Y. Li, *Acc. Chem. Res.*, 2011, **45**, 723-733.
16. G. C. Welch, L. A. Perez, C. V. Hoven, Y. Zhamg, X. D. Dang, A. Sharenko, M. F. Toney, E. J. Kramoer, T. Q. Nguyen and G. C. Banzan, *J. Mat. Chem.*, 2011, **21**, 12700.
17. P. M. Beaujuge and J. M. J. Fréchet, *J Am Chem Soc*, 2011, **133**, 20009-20029.
18. A. Guerrero, N. F. Montcada, J. Ajuria, I. Etxebarria, R. Pacios, G. Garcia-Belmonte and E. Palomares, *J. Mater. Chem. A*, 2013, **1**, 12345-12354.
19. A. Sánchez-Díaz, L. Burtone, M. Riede and E. Palomares, *J. Phys. Chem. C*, 2012, **116**, 16384.
20. A. Sánchez-Díaz, R. Pacios, U. Muñecas, T. Torres and E. Palomares, *Org. Elec.*, 2011, **12**, 329-335.

 This journal is © The Royal Society of Chemistry [year]